

Geophysical Research Letters

RESEARCH LETTER

10.1029/2019GL083680

Key Points:

- SO₂ injections are simulated in different seasons and latitudes in a fully coupled climate model, resulting in a 5 × 4 space of outcomes
- Injections in different seasons lead to different patterns of aerosol optical depth due to differences in the stratospheric circulation
- Injecting only in one season leads to higher global aerosol optical depth than if the same mass were injected over the entire year

Supporting Information:

- Supporting Information S1

Correspondence to:

D. Visioni,
daniele.visioni@cornell.edu

Citation:

Visioni, D., MacMartin, D. G., Kravitz, B., Tilmes, S., Mills, M. J., Richter, J. H., & Boudreau, M. P. (2019). Seasonal injection strategies for stratospheric aerosol geoengineering. *Geophysical Research Letters*, 46. <https://doi.org/10.1029/2019GL083680>

Received 13 MAY 2019

Accepted 21 JUN 2019

Accepted article online 1 JUL 2019

Seasonal Injection Strategies for Stratospheric Aerosol Geoengineering

Daniele Visioni¹ , Douglas G. MacMartin¹ , Ben Kravitz^{2,3} , Simone Tilmes⁴ , Michael J. Mills⁴ , Jadwiga H. Richter⁵ , and Matthew P. Boudreau¹

¹Sibley School for Mechanical and Aerospace Engineering, Cornell University, Ithaca, NY, USA, ²Department of Earth and Atmospheric Sciences, Indiana University, Bloomington, IN, USA, ³Atmospheric Sciences and Global Change Division, Pacific Northwest National Laboratory, Richland, WA, USA, ⁴Atmospheric Chemistry, Observations, and Modeling Laboratory, National Center for Atmospheric Research, Boulder, CO, USA, ⁵Climate and Global Dynamics Laboratory, National Center for Atmospheric Research, Boulder, CO, USA

Abstract Simulations of stratospheric aerosol geoengineering have typically considered injections at a constant rate over the entire year. However, the seasonal variability of both sunlight and the stratospheric circulation suggests seasonally dependent injection strategies. We simulated single-point injections of the same amount of SO₂ in each of the four seasons and at five different latitudes (30°S, 15°S, equator, 15°N, and 30°N), 5 km above the tropopause. Our findings suggest that injecting only during one season reduces the amount of SO₂ needed to achieve a certain aerosol optical depth, thus potentially reducing some of the side effects of geoengineering. We find, in particular, that injections at 15°N or 15°S in spring of the corresponding hemisphere results in the largest reductions in incoming solar radiation. Compared to annual injections, by injecting in the different seasons we identify additional distinct spatiotemporal aerosol optical depth patterns, thanks to seasonal differences in the stratospheric circulation.

1. Introduction

The proposed injection of SO₂ in the stratosphere to partly offset the warming produced by the increase in greenhouse gases [Crutzen, 2006] has received increasing attention in recent years. In the stratosphere SO₂ would oxidize, producing sulfate aerosols which would spread in longitude and latitude, reflecting part of the incoming solar radiation. The response is determined by both the timing and location of the injection, as has been shown for explosive volcanic eruptions (Aquila et al., 2012; Kravitz and Robock, 2011; Pitari et al., 2016; Toohey et al., 2019). For sulfate geoengineering (SG), the response has been shown to depend on the injection location [English et al., 2012; Niemeier & Timmreck, 2015; Tilmes et al., 2017; MacMartin et al., 2017; Jones et al., 2017; Visioni, Pitari, Tuccella, & Curci, 2018], but research has generally not considered the timing of the injection.

Most simulations of SG have focused on strategies where the injection happens at a constant rate throughout the entire year. Until recently most simulations considered equatorial injections (see, e.g., GeoMIP; e.g., Kravitz et al., 2011; Kravitz et al., 2013). This results in strong confinement of the injected aerosols in the tropics, resulting in overcooling the tropics relative to the poles [Kravitz et al., 2016], which also impacts meridional temperature gradients and hence storm tracks [Wang et al., 2018]. Furthermore, the tropical stratospheric heating due to the high tropical aerosol burden could modify the quasi-biennial oscillation (QBO; Aquila et al., 2014; Richter et al., 2017). For this reason, in recent years, simulations with injections placed at different latitudes have been proposed and analyzed [Dai et al., 2018; Tilmes et al., 2017] and have been shown to be capable of achieving more climate objectives than just a global reduction in temperatures [Kravitz et al., 2017; MacMartin et al., 2017; Tilmes, Richter, Kravitz, et al., 2018, accompanied by reduced side effects as compared to equatorial injection.

Here we propose to extend this approach by considering injection rates that vary with the season. There are three main reasons for proposing such a strategy. First, limiting injection to a single season has the potential to increase efficiency (defined as the resulting global-average aerosol optical depth (AOD) per teragram of injected SO₂), because when the injection restarts the next year there would be fewer previously formed particles at that location to coagulate with. This would prevent the aerosol particles from growing too large, hindering their backscattering efficiency [Niemeier & Timmreck, 2015; Pitari et al., 2016] and increasing

their gravitational settling velocity, decreasing their lifetime [Visioni, Pitari, Tuccella, & Curci, 2018]. Second, including the season of injection as an additional degree of freedom to the system, together with location, could increase control of the spatiotemporal pattern of the response, thus increasing the number of climate objectives that could be met simultaneously (Kravitz et al., 2016; MacMartin et al., 2012; MacMartin and Kravitz, 2019). Lastly, the potential to inject less SO₂ to obtain a certain value of optical depth, combined with a greater control of the system, might help to target additional outcomes than temperatures. Reducing the amount of injection would make this approach cheaper and in addition reduce some of the side effects of the stratospheric sulfate burden, such as stratospheric heating and in turn stratospheric dynamic response [Ferraro et al., 2011; Richter et al., 2017] and stratospheric chemistry changes [Visioni et al., 2017; Visioni, Pitari, Tuccella, & Curci, 2018].

There have been a few limited explorations in previous works in regard to injecting at limited times of the year: Heckendorn et al. [2009] first noted that injecting impulsively rather than continuously would reduce the size of the sulfate particles produced. Dai et al. [2018] used a 2-D chemical transport model (with a resolution of ~9.5° latitude per ~1.2-km altitude and a sectional representation for the sulfate particles with 42 bins); while they mainly focused on spatial control of top of the atmosphere (TOA) radiative forcing (RF) via injections at a wide array of latitudes and altitudes, they also simulated injections during December or June at high northern latitudes, determining that some temporal dependence in the RF peak was possible. Kleinschmitt et al. [2018] also simulated a strategy with injections only in two months of the year (April and October), finding that the global RF was 10% more than the case with a yearly injection, while Laakso et al. [2017] did not find significant changes in their RF when shifting the injection season and location in order to follow the maximum solar irradiation.

Our goal is to analyze more comprehensively the possible outcomes of nonconstant injections during the year; this might ultimately lead to injection strategies that build upon and improve the one described by Kravitz et al. [2017]. We start by simulating injections of the same amount of SO₂ one season at a time at five different locations. We then analyze the differences in the resulting temporal and spatial patterns of stratospheric AOD and TOA RF. This provides an initial assessment of the feasibility of a strategy of time-variable injections described above, both by determining if single-point seasonal injections result in an increase in efficiency and whether they produce different solar reduction patterns.

2. Description of Simulations

The simulations have been performed with the Community Earth System Model version 1, with the Whole Atmosphere Community Climate Model as its atmospheric component, CESM1(WACCM), described by Mills et al. [2017], using CLM4.5 as its land model [Tilmes, Richter, Kravitz, et al., 2018]. The model grid is 0.9° latitude × 1.25° longitude, with 70 vertical layers and a model top at 140 km.

Sulfate aerosol microphysics is treated with a three-mode approach [Liu et al., 2012]: While we acknowledge that this approach has its limits in terms of properly simulating the aerosol size distribution, it has been shown to reproduce the outcome of past volcanic eruptions (see Mills et al., 2016, 2017) and thus still offers a good compromise between fidelity and computational burden. The sulfate chemistry mechanisms include SO₂ oxidation into H₂SO₄ and the subsequent formation of sulfate aerosols by nucleation and condensation, followed by coagulation, evaporation, and sedimentation of the formed aerosols.

The baseline simulation (named Base in this paper) is the same one described by Tilmes, Richter, Kravitz, et al. [2018], run under a Representative Concentration Pathway 8.5 emission scenario. For the geoengineering simulations, five injection locations (30°S, 15°S, equator, 15°N, and 30°N) have been selected as in Tilmes et al. (2017), with the sulfate injected roughly 5 km above the tropopause and at a single longitude (180°E). Simulations are performed for injection in each of the four different seasons: December-January-February (DJF), March-April-May (MAM), June-July-August (JJA), and September-October-November (SON), starting in 2040, with 6 Tg SO₂ injected each season (therefore, different seasons have slightly different injection rates per day). Cases with 6 Tg SO₂ injected annually have been also performed for comparison: Results proved to be almost identical to the previous annual cases at the same injection points described in Tilmes et al. [2017; that used CLM4 instead of CLM4.5]. For one of the cases (MAM 15°N) the simulation has been performed for 10 years; based on the results of that simulation, we concluded that the AOD patterns are

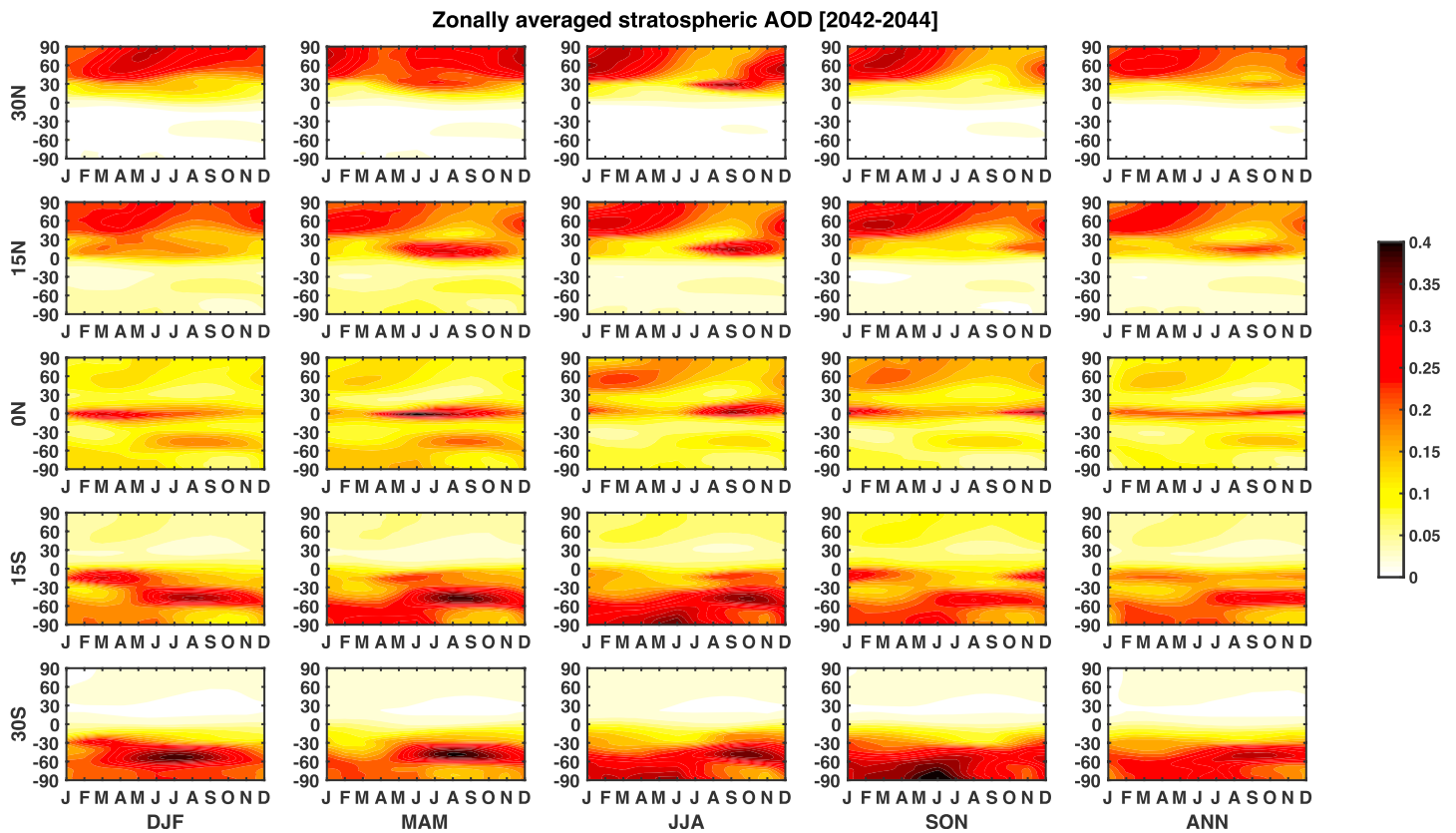


Figure 1. Zonally averaged stratospheric AOD averaged over the three years 2042–2044 as a function of time of year, for all 25 injection scenarios. The values for the individual three years are shown in Figure S3. AOD = aerosol optical depth; DJF = December-January-February; MAM = March-April-May; JJA = June-July-August; SON = September-October-November; ANN = Annual.

already converged by the third year; therefore, all other simulations have been performed for only 5 years and all analyses are performed over the years 2042–2044. We show the full 10 years in the supporting information Figures S1 and S2 (see also MacMartin et al., 2017).

3. Results

3.1. Stratospheric Aerosol

It has been shown using annual injections with CESM1(WACCM) that combining injections at different latitudes has the potential to achieve similar climate goals as combining different solar reduction patterns [Kravitz et al., 2016; Kravitz et al., 2017]. In particular, MacMartin et al. (2017) showed that three different idealized spatial patterns of AOD are achievable using four injection locations (30° and 15° north and south): a uniform pattern (L0), a pattern linearly increasing northward or southward (L1), and a pattern that increases at high latitudes and decreases at tropical latitudes (L2), to manage the overall temperature, the interhemispheric temperature gradient, and the pole-to-equator temperature gradient. The AOD resulting from annually constant injection varies with season due to the Brewer-Dobson circulation in the stratosphere (e.g., Figure 1 in Tilmes et al., 2017; Figure 1 in MacMartin et al., 2017; Figure 3 in MacMartin & Kravitz, 2019), but the above mentioned papers focused only on annual-mean quantities.

In our injection scenarios, the seasonal injection produces temporally and spatially dependent patterns of stratospheric AOD, as shown in Figure 1, that are a product of both the location and the time of the injection; the latter is due to differences in the specific seasonal circulation patterns of the stratosphere. The differences between these patterns and those produced by annual injections of the same amount are reported in Figure 2 a. These changes are defined for each injection as the relative difference $(S_{T,L} - A_L)/A_L$, where $S_{T,L}$ is the $n_{\text{lat}} \times n_{\text{month}}$ matrix containing the monthly 2042–2044 zonal average of the stratospheric AOD at all latitudes

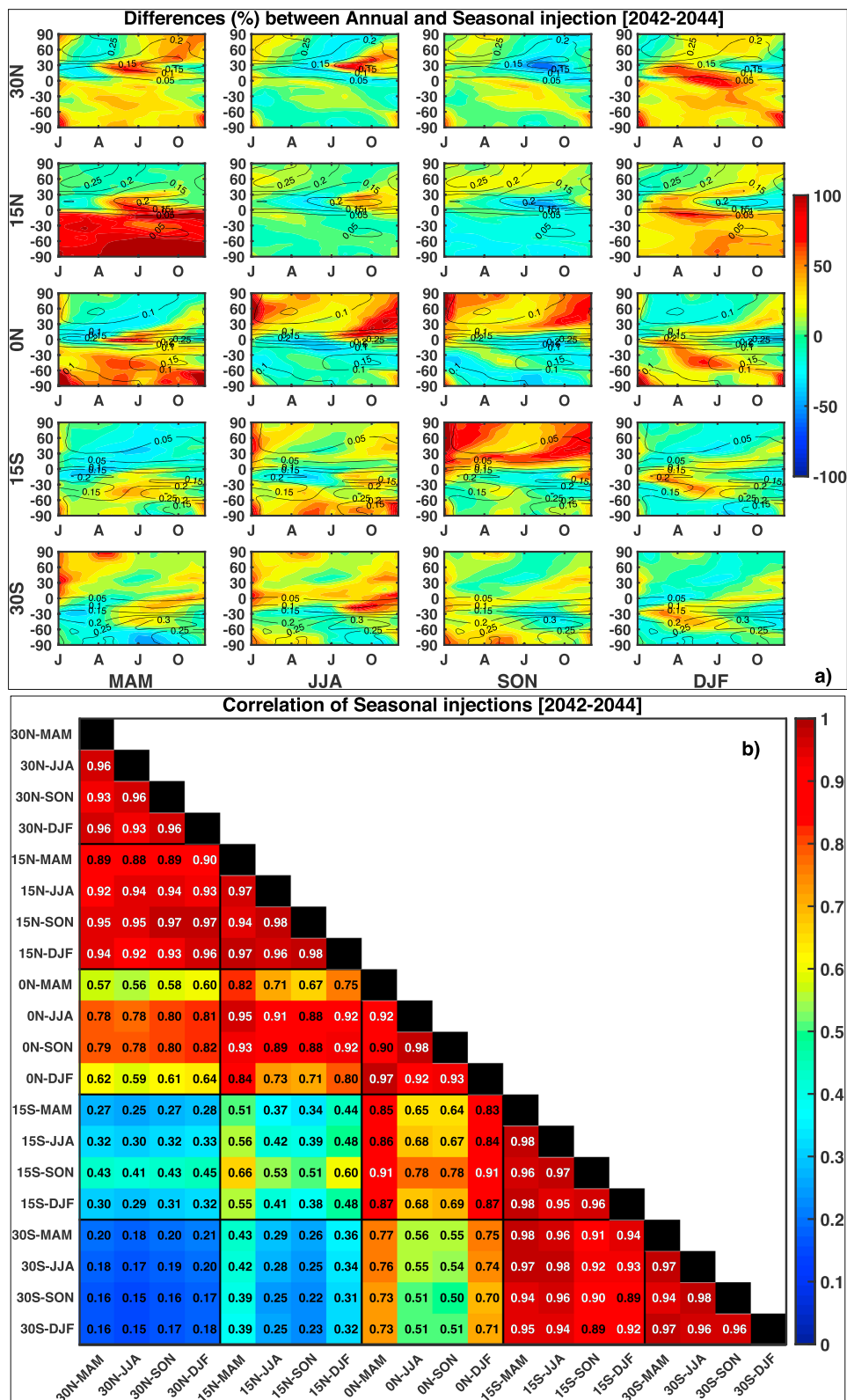


Figure 2. (a) Relative AOD differences (in percent) between the seasonal cases in Figure 1 and the annual case of the same quantity of SO₂ for the same injection location. Black contour lines are for the AOD in the annual scenarios. (b) Correlation matrix of the time-dependent spatial patterns in Figure 1. Since the matrix is symmetrical, only the lower part has been reported for clarity, and the diagonal (where the value is always 1) has been blackened out. AOD = aerosol optical depth; MAM = March-April-May; JJA = June-July-August; SON = September-October-November; DJF = December-January-February.

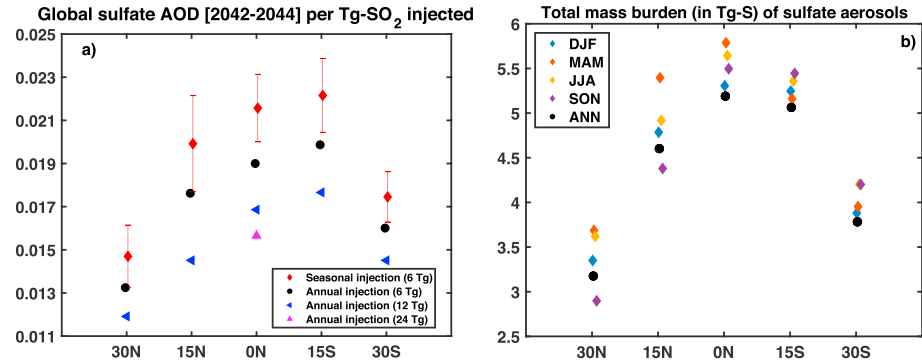


Figure 3. (a) Global sulfate AOD averaged over the years 2042–2044 and normalized by teragrams of SO₂ injected. The colored triangles represent the value for the annual injections described by Tilmes et al. [2017] of 12 and 24 Tg SO₂. Red squares represent the quantity (shown in Figure 1) also averaged over the four different seasonal injection cases at that location, with error bars indicating the range of the four seasonal injections. (b) Total mass burden of SO₄ (expressed in teragrams of sulfur) for the annual injection case (black dots, average over 2042–2044) and for the single injection scenarios (over the same period). AOD = aerosol optical depth; DJF = December–January–February; MAM = March–April–May; JJA = June–July–August; SON = September–October–November; ANN = Annual.

for each season T and injection location L , and A_L is the matrix of the same dimension for the annual injection at the same location L . We also show in Figure 2b the correlations $R_{T_1, L_1}^{T_2, L_2}$ between the AOD for seasonal injections T_1, L_1 and T_2, L_2 in Figure 1, defined as

$$R_{T_1, L_1}^{T_2, L_2} = \frac{\int_{-\pi/2}^{+\pi/2} \int_0^T (S_{T_1, L_1} \times S_{T_2, L_2}) \cos\psi \, d\psi \, dt}{\left[\int_{-\pi/2}^{+\pi/2} \int_0^T S_{T_1, L_1} \cos\psi \, d\psi \, dt \right] \left[\int_{-\pi/2}^{+\pi/2} \int_0^T S_{T_2, L_2} \cos\psi \, d\psi \, dt \right]} \quad (1)$$

where the time integration is over the 36 months of 2042–2044 and spatial integration is over all latitudes (ψ). The resulting matrix shown considers all 20 by 20 possible combinations of cross correlation between the single patterns of monthly and latitudinal dependent AOD between 2042 and 2044 for all locations and seasons and thus provides a measure of the uniqueness of the produced spatiotemporal pattern of AOD at a certain location and season.

The ability to produce independent spatiotemporal patterns of AOD is a necessary prerequisite for producing distinct climate responses, especially in terms of surface air temperatures. As shown in Figures 1 and 2a, differences between the patterns produced by injecting seasonally and annually are indeed present: Changes are always present in the magnitude of the peak of the AOD, and injections at 15° in both hemispheres in the related spring tend to transport more sulfate into the opposite hemisphere, while injections in the related fall tend to be more confined to the same hemisphere of the injection. In some injections, the peak of the AOD is also shifted, especially for injections at 30°. On the other hand, the correlations in Figure 2b show that some spatiotemporal patterns have a correlation close to 1: It can be noted, however, that very high correlations between two patterns do not imply equal outcomes: For the annual injections, the correlation between the 15°N and 30°N injection was 0.92, but the two annual cases clearly produce different climate responses [MacMartin et al., 2017]. In the same way, Figure 2b shows that there are patterns produced with injections in different locations with a correlation very close to 1 (15°N and 30°N, 15°S and 30°S in JJA) that are unlikely to produce a different response, and patterns produced by injecting in the same location but in opposite seasons (for instance, 15°N MAM and SON) that result in lower correlation, thus likely producing different patterns in the surface climate response. Overall, these results might help in reducing the amount of possible combinations in an injection strategy when multiple locations and seasons are combined together in a single simulation.

We now consider the question of efficiency. In Figure 3a we compare stratospheric AOD results obtained for the seasonal injections with both the results for annual injection at the same five location points and with annual injections of 12 and 24 Tg SO₂ (described in Tilmes et al., 2017). The global-mean AOD values (reported also in Figure S4) for the seasonal injections are consistently larger than those for the annual injections by between 6% and 15%, with an average of 9.4%.

It has been established (Kravitz et al., 2019; Niemeier and Timmreck, 2015; Tilmes et al., 2017) that the increase in injection load produces a decrease in AOD per unit of injection (and thus in the scattering efficiency): This happens because coagulation into bigger aerosols is favored for higher stratospheric loads, producing particles that are not as efficient in reflecting sunlight back and have reduced lifetime due to greater sedimentation rates [Visioni, Pitari, Tuccella, & Curci, 2018]. Apart from the influence of the differences in solar insolation and hence the gas phase oxidation of sulfur dioxide to sulfate aerosol, there are no reasons to assume that the operating physical mechanisms responsible for coagulation would be fundamentally different for seasonal injections.

In Figures 3b and S5 we try to understand the previous results by looking at how sulfate aerosol microphysical growth changes in the different cases. In the three-mode approach used in this model configuration [Liu et al., 2012; Mills et al., 2017], particles in the accumulation mode (0.06- to 0.3- μm diameter range) are those with the highest scattering efficiency [Hansen et al., 2005; Pitari et al., 2016]; this information is incorporated into computations of AOD. In Figure 3b we show the global mass burden (in teragrams of sulfur) of sulfate in the 3-year period, while the two modes are shown separately in Figure S5. The total mass burden of SO_4 is higher in spring and summer in the Northern Hemisphere (NH), while less differences are present in the Southern Hemisphere. This is consistent with the behavior of the Brewer-Dobson circulation that strongly controls the transport of chemical species and aerosols from the equator to the poles. In both hemispheres, in spring and summer upward transport at the altitudes of injection is enhanced, thus increasing the overall aerosol lifetime [Tilmes et al., 2017]. This effect is much stronger in the NH, due to topographical differences. When observing the differences in AOD (Figure S4), however, in DJF the global value is higher in the NH than in JJA. This can be explained by looking at the mass burden of just the smaller particles (Figure S5a) that are higher in DJF compared to JJA: This is a result of the increased poleward transport and mixing in winter (Tilmes et al., 2017) that move particles away from the injection location faster and result in fewer preexisting aerosols available for the newly injected SO_2 to coagulate on (increasing their size). This is similar to what was observed in Visioni, Pitari, Tuccella, et al. (2018) in regard to equatorial injections and the QBO: Particles that are more confined due to a specific QBO phase have a higher lifetime but tend to grow too big and thus have smaller optical depth. This is consistent with our initial assumption regarding injecting in a location where fewer aerosols from the previous year are present. Chemical characteristics of the stratosphere at the time of the injection (in particular OH, which oxidizes SO_2), which are heavily dependent on the solar zenith angle (Minschwaner et al., 2011), do not appear to correlate with the resulting SO_4 burden (not shown), indicating that the produced AOD is mostly a function of the transport efficiency.

3.2. TOA RF

In this section we show the resulting TOA RF imbalance, defined as the difference between the net TOA radiative fluxes in the geoengineering simulations and the fluxes in the Base simulations. Given the short duration of our simulations, we limit our analyses to the instantaneous response to the injected aerosol; thus, we only consider the clear-sky TOA fluxes. In this way we can increase the signal-to-noise ratio by eliminating uncertainties and possible changes in cloud coverage due to the stratospheric sulfate [Visioni, Pitari, di Genova, et al., 2018; Schmidt et al., 2018] and focus on the pattern of changes due to the direct effect of sulfate alone. Clear-sky RF, however, is not necessarily an accurate indicator of the effective RF that is commonly used as a metric to assess potential climate change (e.g., Myhre et al., 2013).

In Figures 4a–4e we show the zonal mean distribution in 2042–2044 of TOA RF imbalance, defined as the shortwave (SW) minus longwave TOA fluxes, for the 20 seasonal injections and the annual ones, minus the same quantity for the Base case, thus isolating the effect of the increased sulfate burden. It is clear from the zonal mean distribution of the RF that the biggest driver in terms of the produced pattern is still the injected location rather than the time of the year. However, differences in magnitude are present for different seasons of injection. In Figure 4f we also compare all cases by considering the same quantity globally averaged, the same way it has been done in Figure S2. As is also evident from the zonal AOD patterns in Figure 1, except for equatorial injections, the produced RF is mostly confined (from 70% to 89%) to the same hemisphere where the injection happens. Therefore, when considering an injection strategy with the objective of controlling the interhemispheric temperature gradient (as described by MacMartin et al., 2017), injecting only in seasons where most AOD is confined in the same hemisphere of the injection might be

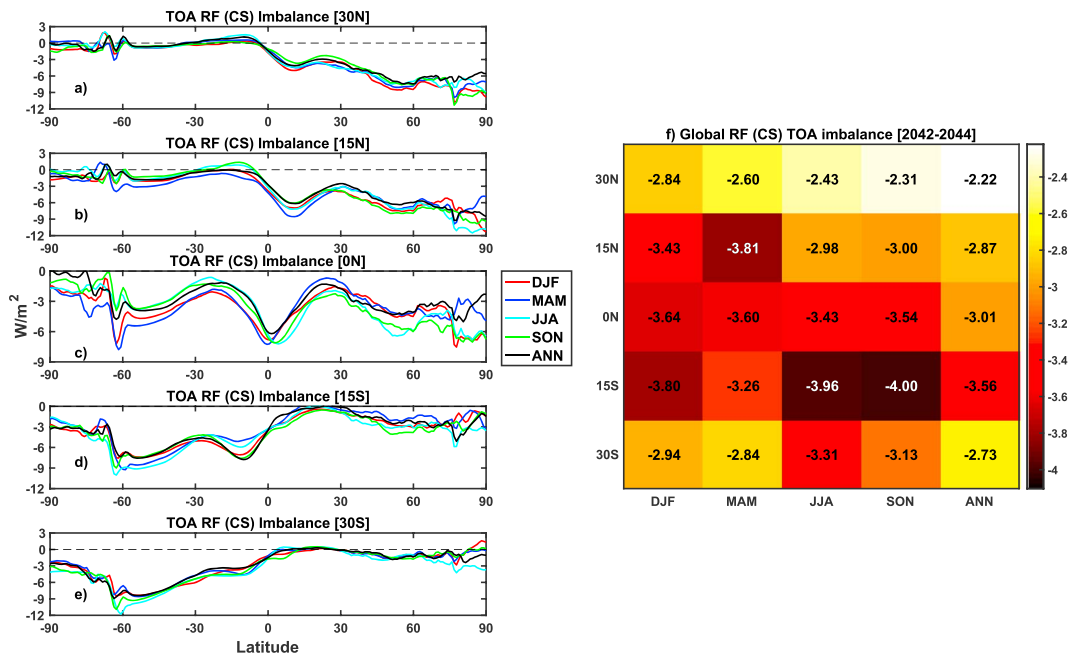


Figure 4. (a–e) Zonal mean of the CS TOA RF imbalance (SW + LW) in 2042–2044 for the five injection locations (one location per panel) and the four seasons, plus the annual case (colors in associated legend). (f) Globally averaged values for the curves shown in panels a–e. CS = clear-sky; TOA = top of the atmosphere; RF = radiative forcing; SW = shortwave; LW = longwave; DJF = December-January-February; MAM = March-April-May; JJA = June-July-August; SON = September-October-November; ANN = Annual.

useful: This is also visible in Figure 2a, where some injections (such as 15°N-SON and 15°S-MAM) show a much stronger hemispheric confinement (up to 80%) as compared to annual injections. To achieve even better confinement, injections may not be placed at fixed latitudes but vary with the location of the jet stream. This could be explored in future studies.

The highest global RF and the highest AOD in Figure S3 do not always match: This can be explained by considering the seasonal differences in incoming solar radiation at different latitudes and by considering when the maximum AOD is reached in the different cases (3 to 4 months after the end of the injection). For instance, at 15°N the highest AOD is produced when injecting in spring, and the corresponding RF is higher than in the other seasons (18%), because the peak is reached in summer. On the other hand, at 30°S the highest AOD is obtained when injecting in spring, but the highest RF is obtained when injecting in winter since the peak AOD is then reached in the summer, two seasons later.

The importance of considering the changes in the annual insolation cycle can also be observed in the differences from annual injections: Global AOD produced via annual injection is always smaller than AOD produced by seasonal injections. On the other hand, there are seasons (SON for 30°N and 15°N, DJF for 15°S and 30°S) where the related TOA imbalance is smaller.

In Figure S6 we also show the latitudinal distribution of the TOA RF imbalance as in Figures 4a–4e, but for each season separately. While the annually averaged RF can inform in regard to the overall resulting surface cooling, injecting seasonally might also alter the seasonal cycle in a different way compared to injecting over the entire year, by cooling more (or less) in certain seasons and locations: Potentially, this could be used to better compensate the mismatch between the CO₂ and the sulfate forcing Govindasamy et al., 2000.

4. Conclusions

In the last decade, many model simulations have been performed to determine how the climate system would respond to the deliberate injection of sulfate or the precursor SO₂ in the stratosphere to mitigate the effect of global warming. The injection strategies in these simulations can vary from constant magnitude equatorial injections to simultaneous injections at different locations to achieve different climate objectives,

as described by Tilmes, Richter, Kravitz, et al. (2018). While this latter approach achieves the specified objectives well and reduces some of the known impacts of SG, some of the impacts produced by global warming are still present (Fasullo et al., 2018; Richter et al., 2017), suggesting room for improving the strategy further. Injections that are also variable in time could potentially improve these results by allowing for further tailoring of the objectives, but before this is included in new simulations strategies, a better understanding of how different injection locations and seasons differently affect the climate is required.

We have presented here a first step in this direction, by analyzing simulations where 6 Tg SO₂ are injected at five different locations (30°N, 15°N, equator, 15°S, and 30°S) in each of the four different seasons. We show that, compared to annually constant injections of the same mass, efficiency can be improved: On average, AOD per unit of injection is 9.4% higher. Injecting in only part of the year allows for more particles to be moved away from the injection location, so that when the injection starts again the following year, SO₂ is injected in a cleaner stratosphere, thus producing new, smaller, and more reflective sulfate aerosol particles rather than condensing onto already present ones. This suggests that injecting SO₂ during the entire year might not be the most efficient strategy and that future simulations should consider strategies that include time-limited injections. We also show that, looking at the TOA SW RF produced by the injected aerosols, there are seasons of injection that produce larger RF: Injections that simply produce larger overall AOD do not necessarily maximize backscattered SW radiation. Rather, maximal SW RF is produced by maximizing stratospheric AOD when the solar irradiance is largest (in the corresponding summer).

Injections in different seasons also produce different spatiotemporal patterns of AOD from annual injections in two main aspects: (1) the temporal location of the peak in the AOD distribution, and its magnitude and (2) the confinement of the AOD in the hemisphere of the injection. The next step would be to understand how these differences translate into changes in the climate response and if they are significant enough to produce further degrees of freedom that can be used to develop a better tailoring of the injection strategy. To do so, longer simulations will be required. The results obtained here will be used in the future to test multiple combinations of seasons and locations to explore the design space of solar geoengineering, possibly for implementation in a feedback algorithm, as was done by Tilmes, Richter, Mills, et al. (2018).

Injecting seasonally may also have the potential to reduce some side effects; this could be explored in future work with longer simulations. In our simulations, for instance, no meaningful changes are apparent in the stratospheric ozone column between annual and seasonal injections (Figure S7). For higher loads, however, net changes in ozone might differ if the peak in the surface area density is reached in a season where its effect on ozone would be smaller (see Tilmes et al., 2009; Tilmes, Richter, Mills, et al., 2018). Other variables might also be affected differently, such as stratospheric heating rates and the changes they produce on atmospheric circulation [Richter et al., 2017] and related quantities. The effect on ecosystems might also differ depending on season of injection: injecting sulfate annually would already affect the seasonal cycle, due to the seasonal differences in the incoming solar radiation [Govindasamy et al., 2000] and since injecting in different season results in seasonally different RF patterns (Figure S6), changes in the seasonal cycle could be amplified or reduced. As Dagon and Schrag [2019] showed (under a solar reduction scenario), changes in the seasonal cycle might be important for vegetation.

The results shown here have been obtained by a single model, using a specific treatment of sulfate microphysics, with all the uncertainties that entails. Although some previous explorations of nonannual injections seem to agree with our results [Kleinschmitt et al., 2018], it would be important to explore with other models the same phase space of locations and seasons to better understand the uncertainties related to sulfate microphysics and its interaction with stratospheric circulation: As projected impacts of geoengineering will depend on design decisions, exploring how different possible choices that could be made affect the climate differently is an important element of ultimately being able to help support informed societal decisions regarding this technology.

References

- Aquila, V., Garfinkel, C. I., Newman, P., Oman, L., & Waugh, D. (2014). Modifications of the quasi-biennial oscillation by a geoengineering perturbation of the stratospheric aerosol layer. *Geophysical Research Letters*, *41*, 1738–1744. <https://doi.org/10.1002/2013GL058818>
- Aquila, V., Oman, L. D., Stolarski, R. S., Colarco, P. R., & Newman, P. A. (2012). Dispersion of the volcanic sulfate cloud from a Mount Pinatubo-like eruption. *Journal of Geophysical Research*, *117*, D06216. <https://doi.org/10.1029/2011JD016968>

Acknowledgments

We would like to acknowledge high-performance computing support from Cheyenne (doi:10.5065/D6RX99HX) provided by NCAR's Computational and Information Systems Laboratory, sponsored by the National Science Foundation. Support for D. V. and D. G. M. was provided by the Atkinson Center for a Sustainable Future at Cornell University and by the National Science Foundation through agreement CBET-1818759. This research was supported in part by the Indiana University Environmental Resilience Institute and the Prepared for Environmental Change grand challenge initiative. The Pacific Northwest National Laboratory is operated for the U.S. Department of Energy by Battelle Memorial Institute under contract DE-AC05-76RL01830. All data used in this article is available at the following link: <http://climate-engineering.mae.cornell.edu/2019/05/03/dataset-visioni-et-al-2019/>

- Crutzen, P. J. (2006). Albedo enhancement by stratospheric sulfur injections: A contribution to resolve a policy dilemma? *Climatic Change*, 77(3-4), 211–220. <https://doi.org/10.1007/s10584-006-9101-y>
- Dagon, K., & Schrag, D. P. (2019). Quantifying the effects of solar geoengineering on vegetation. *Climatic Change*, 153(1-2), 235–251. <https://doi.org/10.1007/s10584-019-02387-9>
- Dai, Z., Weisenstein, D. K., & Keith, D. W. (2018). Tailoring meridional and seasonal radiative forcing by sulfate aerosol solar geoengineering. *Geophysical Research Letters*, 45(2), 1030–1039. <https://doi.org/10.1002/2017GL076472>
- English, J. M., Toon, O. B., & Mills, M. J. (2012). Microphysical simulations of sulfur burdens from stratospheric sulfur geoengineering. *Atmospheric Chemistry and Physics*, 12, 4775–4793. <https://doi.org/10.5194/acp-12-4775-2012>
- Fasullo, J. T., Simpson, I. R., Kravitz, B., Tilmes, S., Richter, J. H., MacMartin, D. G., & Mills, M. J. (2018). Persistent polar ocean warming in a strategically geoengineered climate. *Nature Geoscience*, 11(12), 910–914. <https://doi.org/10.1038/s41561-018-0249-7>
- Ferraro, A. J., Highwood, E. J., & Charlton-Perez, A. J. (2011). Stratospheric heating by potential geoengineering aerosols. *Geophysical Research Letters*, 38, L24706. <https://doi.org/10.1029/2011GL049761>
- Govindasamy, B., Caldeira, K., & Duffy, P. B. (2000). Geoengineering Earth's radiation balance to mitigate CO₂-induced climate change. *Geophysical Research Letters*, 27(14), 2141–2144. <https://doi.org/10.1029/1999GL006086>
- Hansen, J., Sato, M. K. I., Ruedy, R., Nazarenko, L., Lacis, A., Schmidt, G. A., et al. (2005). Efficacy of climate forcings. *Journal of Geophysical Research*, 110, D18104. <https://doi.org/10.1029/2005JD005776>
- Heckendorn, P., Weisenstein, D., Fueglistaler, S., Luo, B. P., Rozanov, E., Schraner, M., et al. (2009). The impact of geoengineering aerosols on stratospheric temperature and ozone. *Environmental Research Letters*, 4(4), 045108. <https://doi.org/10.1088/1748-9326/4/4/045108>
- Jones, A. C., Haywood, J. M., Dunstone, N., Emanuel, K., Hawcroft, M. K., Hodges, K. I., & Jones, A. (2017). Impacts of hemispheric solar geoengineering on tropical cyclone frequency. *Nature Communications*, 8(1), 1382. <https://doi.org/10.1038/s41467-017-01606-0>
- Kleinschmitt, C., Boucher, O., & Platt, U. (2018). Sensitivity of the radiative forcing by stratospheric sulfur geoengineering to the amount and strategy of the SO₂ injection studied with the lmdz-s3a model. *Atmospheric Chemistry and Physics*, 18(4), 2769–2786. <https://doi.org/10.5194/acp-18-2769-2018>
- Kravitz, B., & Robock, A. (2011). Climate effects of high-latitude volcanic eruptions: Role of the time of year. *Journal of Geophysical Research*, 116, D01105. <https://doi.org/10.1029/2010JD014448>
- Kravitz, B., Caldeira, K., Boucher, O., Robock, A., Rasch, P. J., Alterskjaer, K., et al. (2013). Climate model response from the Geoengineering Model Intercomparison Project (GeoMIP). *Journal of Geophysical Research: Atmospheres*, 118, 8320–8332. <https://doi.org/10.1002/jgrd.50646>
- Kravitz, B., MacMartin, D. G., Mills, M. J., Richter, J. H., Tilmes, S., Lamarque, J. F., et al. (2017). First simulations of designing stratospheric sulfate aerosol geoengineering to meet multiple simultaneous climate objectives. *Journal of Geophysical Research: Atmospheres*, 122, 12,616–12,634. <https://doi.org/10.1002/2017JD026874>
- Kravitz, B., MacMartin, D. G., Tilmes, S., Richter, J. H., Mills, M. J., Cheng, W., et al. (2019). Comparing surface and stratospheric impacts of geoengineering with different SO₂ injection strategies. *Journal of Geophysical Research: Atmospheres*, 124, <https://doi.org/10.1029/2019JD030329>
- Kravitz, B., MacMartin, D. G., Wang, H., & Rasch, P. J. (2016). Geoengineering as a design problem. *Earth System Dynamics*, 7(2), 469–497. <https://doi.org/10.5194/esd-7-469-2016>
- Kravitz, B., Robock, A., Boucher, O., Schmidt, H., Taylor, K. E., Stenchikov, G., & Schulz, M. (2011). The Geoengineering Model Intercomparison Project (GeoMIP). *Atmospheric Science Letters*, 12(2), 162–167. <https://doi.org/10.1002/asl.316>
- Laakso, A., Korhonen, H., Romakkaniemi, S., & Kakkola, H. (2017). Radiative and climate effects of stratospheric sulfur geoengineering using seasonally varying injection areas. *Atmospheric Chemistry and Physics*, 17(11), 6957–6974. <https://doi.org/10.5194/acp-17-6957-2017>
- Liu, X., Easter, R. C., Ghan, S. J., Zaveri, R., Rasch, P., Shi, X., et al. (2012). Toward a minimal representation of aerosols in climate models: Description and evaluation in the Community Atmosphere Model CAM5. *Geoscientific Model Development*, 5(3), 709–739. <https://doi.org/10.5194/gmd-5-709-2012>
- MacMartin, D. G., Keith, D. W., Kravitz, B., & Caldeira, K. (2012). Management of trade-offs in geoengineering through optimal choice of non-uniform radiative forcing. *Nature Climate Change*, 3(4), 365–368. <https://doi.org/10.1038/nclimate1722>
- MacMartin, D. G., & Kravitz, B. (2019). Mission-driven research for stratospheric aerosol geoengineering. *Proceedings of the National Academy of Sciences Jan, 201811022*. <https://doi.org/10.1073/pnas.1811022116>
- MacMartin, D. G., Kravitz, B., Tilmes, S., Richter, J. H., Mills, M. J., Lamarque, J. F., et al. (2017). The climate response to stratospheric aerosol geoengineering can be tailored using multiple injection locations. *Journal of Geophysical Research: Atmospheres*, 122, 12,574–12,590. <https://doi.org/10.1002/2017JD026868>
- Mills, M. J., Richter, J. H., Tilmes, S., Kravitz, B., MacMartin, D. G., Glanville, A. A., et al. (2017). Radiative and chemical response to interactive stratospheric sulfate aerosols in fully coupled CESM1(WACCM). *Journal of Geophysical Research: Atmospheres*, 122, 13,061–13,078. <https://doi.org/10.1002/2017JD027006>
- Mills, M. J., Schmidt, A., Easter, R., Solomon, S., Kinnison, D. E., Ghan, S. J., et al. (2016). Global volcanic aerosol properties derived from emissions, 1990–2014, using CESM1(WACCM). *Journal of Geophysical Research: Atmospheres*, 121, 2332–2348. <https://doi.org/10.1002/2015JD024290>
- Minschwaner, K., Manney, G. L., Wang, S. H., & Harwood, R. S. (2011). Hydroxyl in the stratosphere and mesosphere – Part 1: Diurnal variability. *Atmospheric Chemistry and Physics*, 11, 955–962. <https://doi.org/10.5194/acp-11-955-2011>
- Myhre, G., Samset, B. H., Schulz, M., Balkanski, Y., Bauer, S., Bernsten, T. K., et al. (2013). Radiative forcing of the direct aerosol effect from AeroCom Phase II simulations. *Atmospheric Chemistry and Physics*, 13, 1853–1877. <https://doi.org/10.5194/acp-13-1853-2013>
- Niemeier, U., & Timmreck, C. (2015). What is the limit of climate engineering by stratospheric injection of SO₂? *Atmospheric Chemistry and Physics*, 15(16), 9129–9141. <https://doi.org/10.5194/acp-15-9129-2015>
- Pitari, G., Di Genova, G., Mancini, E., Visioni, D., Gandolfi, L., & Cionni, I. (2016). Stratospheric aerosols from major volcanic eruptions: A composition-climate model study of the aerosol cloud dispersal and e-folding time. *Atmosphere*, (6). Retrieved from), 7. <http://www.mdpi.com/2073-4433/7/6/75>
- Richter, J. H., Tilmes, S., Mills, M. J., Tribbia, J. J., Kravitz, B., MacMartin, D. G., et al. (2017). Stratospheric dynamical response and ozone feedbacks in the presence of SO₂ injections. *Journal of Geophysical Research: Atmospheres*, 122, 12,557–12,573. <https://doi.org/10.1002/2017JD026912>

- Schmidt, A., Mills, M. J., Ghan, S., Gregory, J. M., Allan, R. P., Andrews, T., et al. (2018). Volcanic radiative forcing from 1979 to 2015. *Journal of Geophysical Research: Atmospheres*, *123*, 12,491–12,508. <https://doi.org/10.1029/2018JD028776>
- Tilmes, S., Garcia, R. R., Kinnison, D. E., Gettelman, A., & Rasch, P. J. (2009). Impact of geoengineered aerosols on the troposphere and stratosphere. *Journal of Geophysical Research*, *114*, D12305. <https://doi.org/10.1029/2008JD011420>
- Tilmes, S., Richter, J. H., Kravitz, B., MacMartin, D. G., Mills, M. J., Simpson, I. R., et al. (2018). CESM1(WACCM) stratospheric aerosol geoengineering large ensemble (GLENS) project. *Bulletin of the American Meteorological Society*, *99*(11), 2361–2371. <https://doi.org/10.1175/BAMS-D-17-0267.1>
- Tilmes, S., Richter, J. H., Mills, M. J., Kravitz, B., MacMartin, D. G., Garcia, R. R., et al. (2018). Effects of different stratospheric SO₂ injection altitudes on stratospheric chemistry and dynamics. *Journal of Geophysical Research: Atmospheres*, *123*, 4654–4673. <https://doi.org/10.1002/2017JD028146>
- Tilmes, S., Richter, J. H., Mills, M. J., Kravitz, B., MacMartin, D. G., Vitt, F., et al. (2017). Sensitivity of aerosol distribution and climate response to stratospheric SO₂ injection locations. *Journal of Geophysical Research: Atmospheres*, *122*, 12,591–12,615. <https://doi.org/10.1002/2017JD026888>
- Toohay, M., Krüger, K., Schmidt, H., Timmreck, C., Sigl, M., Stoffel, M., & Wilson, R. (2019). Disproportionately strong climate forcing from extratropical explosive volcanic eruptions. *Nature Geoscience*, *12*(2), 100–107. <https://doi.org/10.1038/s41561-018-0286-2>
- Visioni, D., Pitari, G., Aquila, V., Tilmes, S., Cionni, I., Di Genova, G., & Mancini, E. (2017). Sulfate geoengineering impact on methane transport and lifetime: Results from the Geoengineering Model Intercomparison Project (GeoMIP). *Atmospheric Chemistry and Physics*, *17*(18), 11,209–11,226. <https://doi.org/10.5194/acp-17-11209-2017>
- Visioni, D., Pitari, G., di Genova, G., Tilmes, S., & Cionni, I. (2018). Upper tropospheric ice sensitivity to sulfate geoengineering. *Atmospheric Chemistry and Physics*, *18*(20), 14,867–14,887. <https://doi.org/10.5194/acp-18-14867-2018>
- Visioni, D., Pitari, G., Tuccella, P., & Curci, G. (2018). Sulfur deposition changes under sulfate geoengineering conditions: quasi-biennial oscillation effects on the transport and lifetime of stratospheric aerosols. *Atmospheric Chemistry and Physics*, *18*(4), 2787–2808. <https://doi.org/10.5194/acp-18-2787-2018>
- Wang, Q., Moore, J. C., & Ji, D. (2018). A statistical examination of the effects of stratospheric sulfate geoengineering on tropical storm genesis. *Atmospheric Chemistry and Physics*, *18*(13), 9173–9188. <https://doi.org/10.5194/acp-18-9173-2018>